Journal of Solid State Chemistry 182 (2009) 2053–2060

Contents lists available at ScienceDirect

Journal of Solid State Chemistry

journal homepage: www.elsevier.com/locate/jssc

$VNb_9O_{25-\delta}$—Synthesis, electrical conducting behaviour and density functional theory (DFT) calculation

Carina Bergner [a], Vladimir Vashook [a], Stefano Leoni [b], Hubert Langbein [a,*]

[a] Fachrichtung Chemie und Lebensmittelchemie, Technische Universität Dresden, Helmholtz Str. 10, D-01069 Dresden, Germany
[b] Max-Planck-Institut für Chemische Physik fester Stoffe, Nöthnitzer Str. 40, D-01187 Dresden, Germany

ARTICLE INFO

Article history:
Received 12 February 2009
Received in revised form
29 April 2009
Accepted 3 May 2009
Available online 18 May 2009

Keywords:
Vanadates
Niobates
Chemical synthesis
Electrical properties
DFT calculation

ABSTRACT

In order to investigate the influence of the oxygen partial pressure ($p(O_2)$) on the electrical conductivity, VNb_9O_{25} was prepared by thermal decomposition of freeze-dried oxalate precursors and by a solid state reaction of V_2O_5/Nb_2O_5 mixtures. The samples were characterised by X-ray diffraction, grain size analysis and scanning electron microscopy (SEM). The electrical conductivity of the *n*-type semiconductor $VNb_9O_{25-\delta}$ can be interpreted as an activated hopping process with a preferred localisation of charge carriers at V(IV) centres. The electronic structure of $VNb_9O_{25-\delta}$ was calculated within the framework of the local density approximation (LDA) to DFT. Partial reduction of V(V) centres causes localised vanadium states to appear inside the band gap. The calculated activation energy values are in good agreement with the experimental ones.

1. Introduction

Vanadium and niobium oxides are well investigated with emphasis on its catalysis and electrochemical applications [1–3]. Mixed oxides of the quasi-binary system V_2O_5–Nb_2O_5 promise catalytic selectivity [4,5] due to the partially reducible V_2O_5 embedded into the hardly reducible but selective Nb_2O_5 [5,6]. Examples of catalytic reactions are the selective oxidation of propane to acrolein over supported V_2O_5/Nb_2O_5 catalysts [4] and the propane oxidative dehydrogenation reaction to propene catalysed by V_2O_5/Nb_2O_5 mixed metal oxides and supported metal oxides [5,7,8].

VNb_9O_{25} is the only known thermodynamically stable phase of the quasi-binary system V_2O_5–Nb_2O_5 [9]. It was synthesised for the first time in 1960 by a solid state reaction (SSR) [10]. Its structure was determined by consideration of isostructural compounds [11], such as PNb_9O_{25} [12], and later refined by single crystal data analysis [13]. The structure of VNb_9O_{25} consists of 3×3 blocks of $[NbO_6]$-octahedra linked by corner-sharing $[VO_4]$ tedrahedra. A low temperature modification, which is obtained via sol–gel synthesis at 600 °C, is known to be a solid solution of 10% V_2O_5 in TT–Nb_2O_5, the low ("tief") temperature modification of Nb_2O_5 [14]. The transformation TT → VNb_9O_{25} is irreversible suggesting that this TT modification is metastable. Recently, we were able to synthesise a further metastable VNb_9O_{25} phase via a special sol–gel process from alkoxides [15].

Besides VNb_9O_{25} there are two further phases known in the quasi-binary system V_2O_5–Nb_2O_5 with the compositions $V_2Nb_9O_{27,5}$ [14] and $VNbO_5$ [16]. Both are metastable and can be synthesised via precursor decomposition at low temperatures between 500 and 700 °C. Their decomposition into VNb_9O_{25} and V_2O_5 starts above 750 °C [14,16]. It was shown recently that all the hitherto known phases in the V_2O_5–Nb_2O_5 system can be synthesised in a relatively simple manner by thermal decomposition of freeze-dried solutions of ammonium oxo-oxalato-niobate and ammonium vanadate [17].

The phase formation process conducted at low temperatures modifies the sample morphology compared to a sintered sample of equal composition. This pertains not only to a varying particle size distribution, but also to altered grain boundary properties. Both features are thought to influence the electrical characteristics of VNb_9O_{25} after synthesis via a soft-chemistry route (SCR) [18]. Although the conductivity mechanisms of V_2O_5 and Nb_2O_5 as well as their oxygen partial pressure ($p(O_2)$) dependency are well investigated [1,3,19], details on the electrical behaviour of VNb_9O_{25} are not reported thus far.

To investigate the influence of $p(O_2)$ on the electrical conductivity, VNb_9O_{25} was prepared via decomposition of a freeze-dried mixture of oxo-oxalato-niobate(V) and oxo-oxalato-vanadate(IV). In addition, a solid state reaction was used to synthesise VNb_9O_{25} in order to compare the dependence of physical and chemical properties on the synthetic pathway.

* Corresponding author. Fax: +49 351 46337287.
E-mail address: Hubert.Langbein@chemie.tu-dresden.de (H. Langbein).

0022-4596/$ - see front matter © 2009 Elsevier Inc. All rights reserved.
doi:10.1016/j.jssc.2009.05.015

Conductivity measurements were performed along with temperature-dependent oxygen-loss measurements in a temperature range from 300 to 800 °C. From these measurements the activation energy was determined and compared with DFT-LDA electronic structure calculations.

2. Experimental

2.1. Sample preparation

Unconventional synthesis of VNb_9O_{25} was performed via the freeze-drying method. Aqueous solutions of oxo-oxalato-vanadate(IV) (V_2O_5 in oxalic acid, molar ratio $V^{5+} : C_2O_4^{2-} = 1 : 2.5$) and oxo-oxalato-niobate(V) (amorphous Nb_2O_5 in oxalic acid, molar ratio $Nb^{5+} : C_2O_4^{2-} = 1 : 3$) of composition V:Nb = 1:9 (pH = 1.5) were frozen to liquid nitrogen temperature. The frozen mixture was dried in a vacuum chamber of an Alpha 2-4 freeze-drying apparatus (Christ) at a pressure of 0.020–0.040 mbar from −33 to 17 °C. The resulting water-soluble powder was pre-decomposed by heating at a rate of 5 K/min up to 350 °C, and keeping it for 30 min at this temperature. The subsequent phase formation was carried out for 5 h at a temperature of 1000 °C.

To assess whether any oxalic acid might get lost during the freeze-drying process (see Section 3.1), the behaviour of free oxalic acid under vacuum atmosphere was studied as well. To this end, a 0.1 M oxalic acid was freeze-dried using similar conditions as described above.

The thermal decomposition of niobium-free oxo-oxalato-vanadate(IV) and vanadium-free oxo-oxalato-niobate(V) was investigated with respect to potentially cumulative effects.

In order to prepare VNb_9O_{25} by solid state reaction, a mixture of vanadium and niobium oxide V_2O_5:Nb_2O_5 = 1:9 was annealed for 24 h at 1000 °C on air. Two different species Nb_2O_5 were used: a freshly precipitated amorphous Nb_2O_5 and its high temperature H modification.

2.2. Sample characterisation

The content of oxalic acid and of the vanadium(IV) species within the freeze-dried product was determined by manganometric titration. Oxo-oxalato-vanadate(IV)–oxo-oxalato-niobate(V) mixtures were dissolved in 5% sulphuric acid. After heating the solutions for 10 min in the presence of Na_2SO_3, they were titrated with 0.02 M $KMnO_4$ solution.

Differential thermal analysis (DTA) and thermogravimetry (TG) were performed by means of a Netzsch STA 409 PC-Luxx analyser coupled with a quadrupole mass spectrometer QMG 420 (Balzers).

X-ray powder diffraction was carried out on a Siemens D5000 X-ray diffractometer using Cu$K\alpha_1$/$K\alpha_2$-radiation. Data were collected for 1 h within a $20^\circ \leq 2\theta \leq 80^\circ$ range.

For the determination of the particle size distribution by dynamic light scattering (DLS) a particle size analysator LS230 (Beckmann Coulter) was utilised. The three-cycle measurements (5 min) of the samples dispersed in a 0.1% $Na_4P_2O_7$ solution were carried out after a 5 min supersonic pre-treatment.

The specific surface measurements were conducted by the Brunauer–Emmett–Teller method (BET) with nitrogen (device calibration with helium gas) using a SA 3100 apparatus (Beckmann Coulter).

IR absorption spectra were measured on a BioRad Excalibur FTS 3000.

Scanning electron microscopy (SEM) was performed on a Philips XL30 apparatus, using a LaB_6-cathode and an acceleration voltage of 25 kV.

The temperature-dependent oxygen loss ($p(O_2)$ measurement) was controlled in a tube furnace with oxygen-sensitive sensors at each port. Samples were heated in steps of 100 K up to 1000 °C while an inert gas flow (nitrogen with $p(O_2) = 20$ Pa or argon with $p(O_2) = 620$ Pa) was maintained. After each step the system was allowed to thermally equilibrate before resuming the heating programme [20].

The electrical conductivity was measured using the direct current (DC) four-point method. Therefore two current and two potential platinum leads were sintered into a pill of VNb_9O_{25} for 5 h at 950 °C in oxygen atmosphere. The density of the ceramic pill of the SCR sample is $d = 2.517$ g/cm^3 (porosity 44.8%); the density of the SSR ceramic sample is $d = 2.754$ g/cm^3 (porosity 39.6%). Before evaluation, the conductivity results were corrected for sample porosity as given in [21].

Heating and cooling processes were carried out with rates of 6 K/min and the maximum temperature of 800 °C was held for 1 h. All measurement cycles were repeated at least twice under the same experimental conditions before the $p(O_2)$ was changed. To investigate the adjustment to equilibration at 800 °C, an additional measurement in air with a dwell time of 5 h was included.

3. Results and discussion

3.1. Decomposition of the freeze-dried samples

As for trisammonium-oxo-trisoxalato-niobate [22], the decomposition of freeze-dried ammonium-free oxo-oxalato-vanadate(IV), oxo-oxalato-niobate(V) and of their mixtures takes place in three major steps: (I) vaporisation of crystal water between 85 and 130 °C; (II) decomposition of oxalate by a quick release of CO, CO_2 and chemically bound H_2O from 140 to 200 °C; and (III) a slow release of CO and CO_2 from 200 to 330 °C (350 °C for oxo-oxalato-vanadate(IV)). This is evidenced by the mass spectroscopic analysis of the gaseous decomposition products. The mass loss of 3–5% at temperatures between 350 and 1000 °C in argon, and at about 600 °C in air, displays the low remaining carbon concentration of the pre-decomposed powders of Nb_2O_5 and VNb_9O_{25} after heating in air (Fig. 1, Table 1). All in all, a heating process in air results in compounds with stable compositions above 600 °C, while a treatment in argon leads to a higher mass loss in case of V_2O_5 (which is reduced to V_2O_{3+x}), and to a reduced mass loss for Nb_2O_5 and VNb_9O_{25} because of the higher residual carbon concentrations.

The freeze-dried powders of the oxo-oxalato-metallates are hygroscopic. This can be observed by an increasing agglomeration and discolouring of the samples after storage in ambient air. The content of crystal water strongly depends on the dwell time and the conditions during the freeze-drying process as well as on the sample storage. A freshly prepared sample of the 1:9 mixture contains less water than a few weeks old sample (Table 1). An analysis of the remaining compounds after the heating process in air coupled with the results of the manganometric titration is presented in Table 1. Surprisingly, the averaged ratio between metal atoms and oxalate ions for the 1:9 mixture is 1:2.3 instead of 1:2.9, as expected from the composition of the precursor solution. The loss of oxalate probably results from oxalic acid in the initial precursor solution according to equilibrium (1) [23]:

$$H_3NbO(C_2O_4)_3 + 2H_2O \rightleftarrows H_2NbO(OH)(C_2O_4)2H_2O + H_2C_2O_4 \quad (1)$$

Oxalic acid completely sublimates under the chosen freeze-drying conditions within 30 h [24].

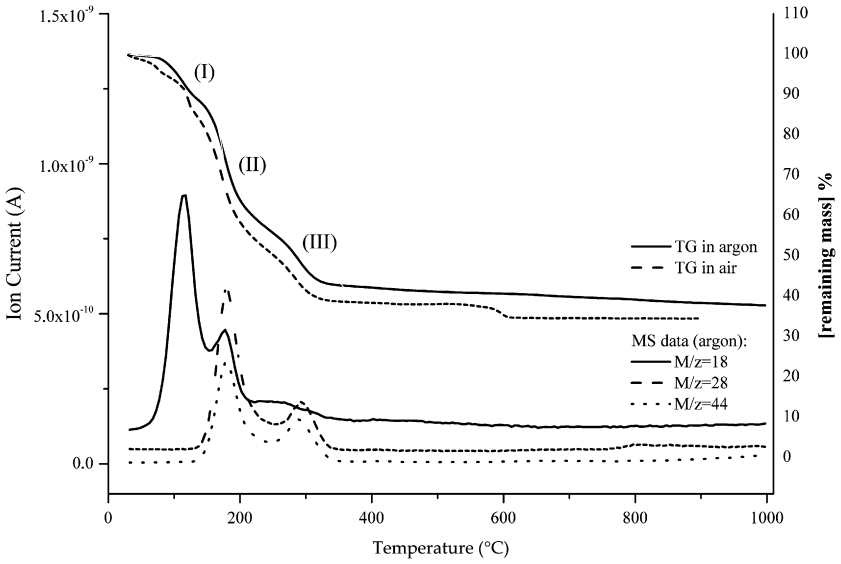

Fig. 1. Thermal analysis and mass spectroscopic analysis of a freeze-dried 1:9 mixture of oxo-oxalato-vanadate (IV) and oxo-oxalato-niobate(V). Heating rate 5 K/min, atmosphere: argon.

Table 1
(DTA)-TG-(MS) data of the oxo-oxalato-vanadate(IV), oxo-oxalato-niobate(V) and a 1:9 mixture of both (two samples: (a) after one month storage and (b) freshly prepared) and calculated ratio of metal atoms and oxalic acid (M^{n+} : $C_2O_4^{2-}$).

	Oxo-oxalato-vanadate(IV)	Oxo-oxalato-niobate(V)	1:9 mixture	
			(a)	(b)
(DTA)-TG				
Remaining				
Compound (°C) in air	V_2O_5 (800)	Nb_2O_5 (1000)	VNb_9O_{25} (1000)	
Mass in air	34.5%	31.8%	34.3%	38.0%
(DTA)-TG-(MS)			(a)	(b)
Remaining				
Compound (°C) in argon	V_2O_3 (800)	Nb_2O_5, CO_x (1000)	VNb_9O_{25}, CO_x (1000)	
Mass in argon	27.3%	36.7%	37.7%	36.9%
Mass loss $M^+ = 18$ till 130 °C in argon	11.8%	9.9%	10.8%	6%
M^{n+} : $C_2O_4^{2-}$	1:1.8	1:2.9	1:2.2	1:2.3

3.2. Phase formation of mixed oxides

The TT modification of VNb_9O_{25} can be obtained by the decomposition of the freeze-dried oxo-oxalato complexes up to 600 °C [14].

X-ray powder diffractometry of VNb_9O_{25} synthesised at 1000 °C via SCR or SSR results basically in identical diffraction patterns which agree well with literature data [15,18]. However, there are slight but significant differences in the IR absorption spectra of the VNb_9O_{25} samples. While the SCR leads to an additional IR absorption at about 930 cm^{-1} (which is in agreement with literature data for the sol–gel method [25]) the SSR results in two additional absorptions at about 550 and 730 cm^{-1}, also observed before [26]. This difference may hint at mixed occupation of the metal sites within the structure of VNb_9O_{25}.

3.3. Particle characterisation

Particles synthesised from V_2O_5 and H–Nb_2O_5 by SSR have diameters ranging from 1 to 30 μm, with a mean value of about 6.5 μm (Fig. 2). The particle sizes of the major part of VNb_9O_{25}

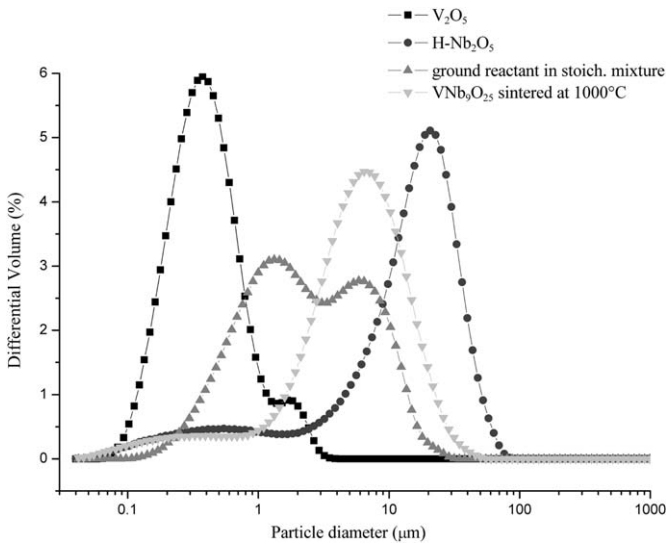

Fig. 2. Particle size distribution of VNb_9O_{25} synthesised via solid state reaction and its educts: V_2O_5, H–Nb_2O_5 and the ball milled mixture.

synthesised via SCR at 1000 °C range from 1 to 40 μm with a maximum at about 6.2 μm (Fig. 3). However, there is also a significant fraction of smaller particles with diameters from 45 nm to 1 μm and a second maximum in the particle size distribution at about 340 nm. A similar bimodal distribution with a slight shift of the maxima (260 nm, 8.9 μm) was determined for TT–VNb_9O_{25} (after decomposition at 600 °C). The particle size distribution of the pre-decomposed amorphous powder lies between 1 and 200 μm, with a maximum at 79 μm. In this case, highly porous soft agglomerated powders of small amorphous primary particles are found. On annealing at 600 °C a shrinkage takes place and crystallisation processes result in a lowering of the specific surface area. This process continues during the transformation to the thermodynamically stable form at 1000 °C and a further light decrease of the average particle size is observed. Simultaneously, a grain growth of the small primary particles begins. This results in a light increase of the average particle size in the lower part of the particle size distribution. The specific surface area is about 20 m^2/g for TT–VNb_9O_{25} (SCR, 600 °C) and 2 m^2/g for VNb_9O_{25} (SCR, 1000 °C).

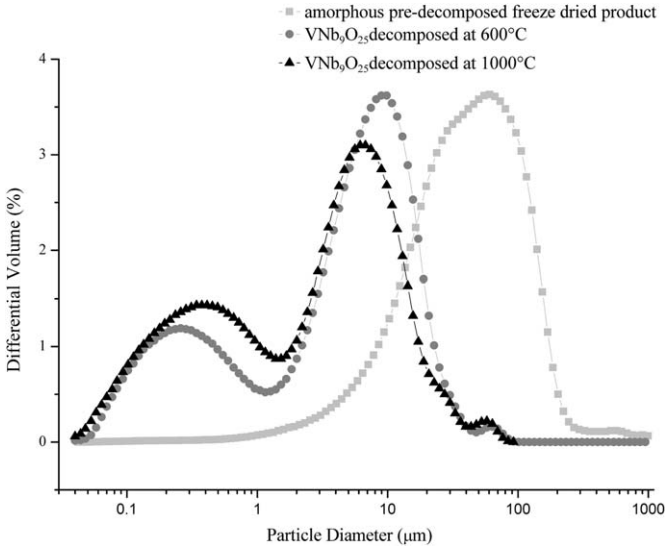

Fig. 3. Particle size distribution of VNb_9O_{25} synthesised via soft chemistry route: pre-decomposed amorphous freeze-dried product, product after sintering at 600 °C with TT–Nb_2O_5 structure, and after sintering at 1000 °C.

Scanning electron micrographs of the differently prepared samples of VNb_9O_{25} display either small and compact crystals (if prepared by the SSR route) or long, thin needles for the SCR one (Fig. 4). Nevertheless, there is no significant difference for samples synthesised by SSR from H–Nb_2O_5 or from freshly precipitated Nb_2O_5 apart from the presence of some larger molten blocks of long needles in case of samples made by the SSR route from H–Nb_2O_5. It cannot be excluded that the bimodal grain size distribution of the SCR samples (Fig. 3) is partially caused by the large aspect ratio of the needles.

The liquid starting mixture of the metal complexes used in the SCR yields first a well homogenised freeze-dried powder of the oxo-oxalato complexes which decomposes during the pre-decomposing process into loose, reactive aggregates of small amorphous particles. The crystallisation process takes place between 500 and 600 °C and yields a solid solution of V_2O_5 in Nb_2O_5 with the structure of TT–Nb_2O_5. Between 600 and 1000 °C this metastable phase is transformed to VNb_9O_{25}. During the whole crystallisation process of the needle-shaped crystals the presence of a molten phase can be excluded. In the case of SSR the starting powder is a less reactive mixture of single oxides. Because of the relatively low melting temperature of V_2O_5 the presence of a liquid phase during the (in all likelihood direct) phase formation process cannot be excluded. This could explain the crystallisation of the more compact crystals. While the use of freshly precipitated Nb_2O_5 in case of SSR results in a homogeneous particle size distribution (Fig. 4) caused by a higher reactivity of the starting mixture, the less reactive powder with H–Nb_2O_5 might contain larger areas of molten V_2O_5 during the phase formation process, which supports the crystallisation of some larger crystal blocks.

3.4. Temperature-dependent oxygen loss

Oxygen release of samples prepared by SCR is investigated during the heating process in an oxygen-depleted atmosphere (Fig. 5). VNb_9O_{25} as well as its TT modification releases oxygen during a heating process and takes it up again during the

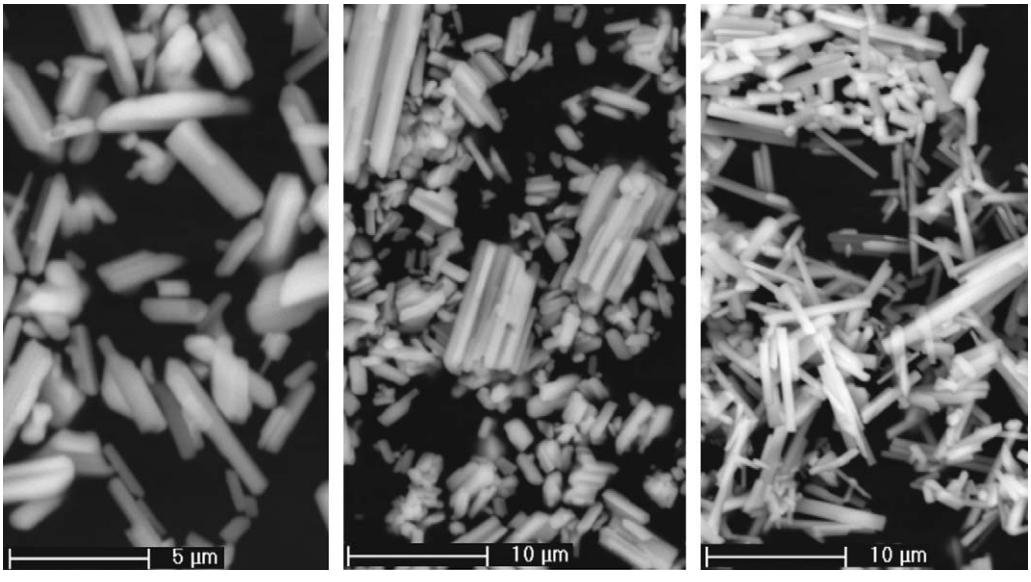

Fig. 4. Scanning electron micrograph (BSE detector, 25 kV) of VNb_9O_{25} annealed at 1000 °C (from left to right): SSR with freshly precipitated Nb_2O_5, SSR with H–Nb_2O_5 and SCR.

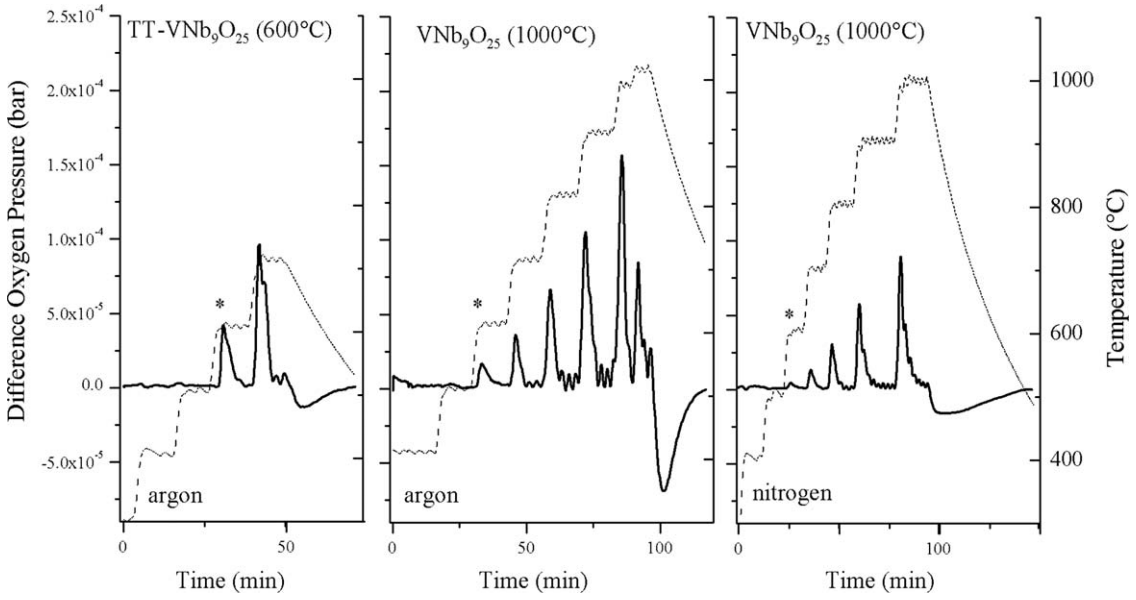

Fig. 5. Temperature dependent oxygen loss of TT–VNb_9O_{25} (SCR, 600 °C) and VNb_9O_{25} (SCR, 1000 °C) in argon ($p(O_2) = 620$ Pa), as well of VNb_9O_{25} (SCR, 1000 °C) in nitrogen ($p(O_2) = 20$ Pa), * marked begin of the oxygen release at 600 °C.

subsequent cooling process, without phase transformation. However, the process is not completely reversible during the relatively fast cooling process, as confirmed by a slight mass loss. About 1.4% of the absolute oxygen content in argon, and 5.8% in nitrogen, gets irreversibly lost. The oxygen release starts between 500 and 600 °C in each case. The oxygen-poorer nitrogen flow leads to an extended release at each temperature step of the heating process as well as to a delayed refill during the cooling step. Overall, VNb_9O_{25} exhibits a "breath-like" behaviour at temperatures above 600 °C in oxygen-reduced atmospheres according to its equilibrium (2):

$$V^{5+}Nb_9^{5+}O_{25} \rightleftarrows V_{1-\delta}^{5+}V_{\delta}^{4+}Nb_9^{5+}O_{25-\delta/2} + \delta/4O_2; V^{4+} = e^- \quad (2)$$

3.5. Electrical conductivity

The conductivity measurements of $VNb_9O_{25-\delta}$ exhibit the characteristics of a semiconductor. The absolute values vary between 1×10^{-7} S/cm at about 400 °C in air to 1×10^{-2} S/cm at about 800 °C in reduced oxygen atmosphere.

Since the equilibration is retarded after each $p(O_2)$ change, data analysis was carried out for each second cooling process only. $VNb_9O_{25-\delta}$ is an *n*-semiconductor because its conductivity at constant temperature decreases with increasing $p(O_2)$. A similar behaviour of samples prepared by the SSR route (Fig. 6) and the SCR one (Fig. 7) is observed. Slight differences of the absolute conductivity values of both samples are due to a different thickness of the sintered pills which determines the oxygen release and refill.

The thermal activated mobility of the available charge carriers dominates the temperature dependence of the conductivity below 600 °C. The activation energies for the total electrical conductivity in this low temperature interval (calculated from the slope of the Arrhenius plot below 600 °C) range from 80 to 97 kJ/mol for SCR samples and SSR samples, respectively (Table 2). Due to the high activation energy of ion diffusion in the solid, an oxygen deficiency change practically does not take place in this temperature interval. Above 600 °C, a $p(O_2)$ dependent oxygen release results in an increase of the charge carrier concentration,

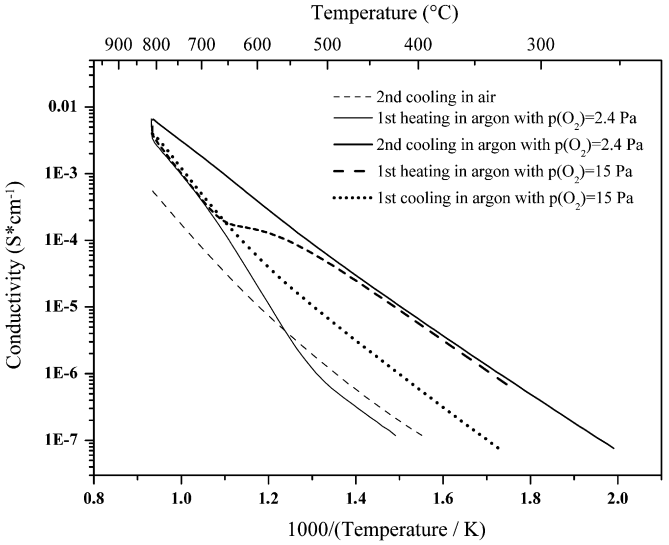

Fig. 6. Temperature dependent conductivity of VNb_9O_{25} synthesised via SSR; the sequence of sample marking corresponds to the sequence of measurements.

which is associated with the reduction of the corresponding amount of vanadium(V) to vanadium(IV). For measurements with $p(O_2) \geq 15$ Pa this leads to a remarkably high increase of the conductivity with increasing temperature, and the activation energies for the total electrical conductivity (calculated from the slope of the Arrhenius plot between 600 and 800 °C) take values between 130 and 148 kJ/mol (Table 2).

For $p(O_2) \geq 15$ Pa and temperatures above 600 °C a relatively fast equilibration of the oxygen content takes place. This can be concluded from (i) the nearly identical heating and cooling curves of a second measurement cycle in air (Fig. 7) and (ii) from the course of the heating curve at $p(O_2) = 5$ Pa after cooling the sample at $p(O_2) = 2.4$ Pa (Fig. 6). Because of the frozen oxygen content after cooling at $p(O_2) = 2.4$ Pa and the resultant non-equilibrium concentration of V(IV), the heating curve at $p(O_2) = 15$ Pa follows the course of the preceding cooling curve at $p(O_2) = 2.4$ Pa up to about 500 °C. Between 500 and 650 °C, the

slope of the curve obtained at $p(O_2) = 15$ Pa decreases because of the onset of oxygen uptake. Above 700 °C the equilibration is completed and the curve compares nicely with the subsequent cooling curve at $p(O_2) = 15$ Pa in this temperature range. For $p(O_2) < 15$ Pa the equilibration at certain temperatures requires considerable time, and even after 5 h it is not fully achieved. Nonetheless, the conductivity saturates at a constant value within 5 h. Here, the slight differences after one and after 5 h can be considered insignificant. This behaviour can be inferred from the heating curves at $p(O_2) = 2.4$ Pa for the SSR sample, and at $p(O_2) = 6$ Pa for the SCR sample, after heating and cooling in air in each case. In spite of the low $p(O_2)$, up to about 500 °C conductivity values are observed, which are typically obtained for samples in air atmosphere. Above 500 °C the remarkably high increase of the conductivity with increasing temperature is caused by the release of oxygen. But, unlike the behaviour at higher $p(O_2)$, a dwell time of at least 1 h at 800 °C is required to reach an approximate equilibrium state. A further increase of the conductivity up to the starting value of the subsequent cooling curve is observed. A non-sufficient dwell time could be the reason for the nonlinear course of the cooling curve of the SCR sample at $p(O_2) = 6$ Pa between 800 and 650 °C (Fig. 7). Additional measurements of the titration current during the conductivity measurements and the calculation of the change of oxygen content confirm the described retarded loss and uptake of oxygen. Fig. 8 shows the results for a SSR sample annealed at 900 °C and cooled to room temperature in air atmosphere with a rate of 4 K/min. During the first heating process at $p(O_2) = 2.4$ Pa a quick release of oxygen takes place. An uptake of oxygen during the cooling process with a significant change of the oxygen content takes only

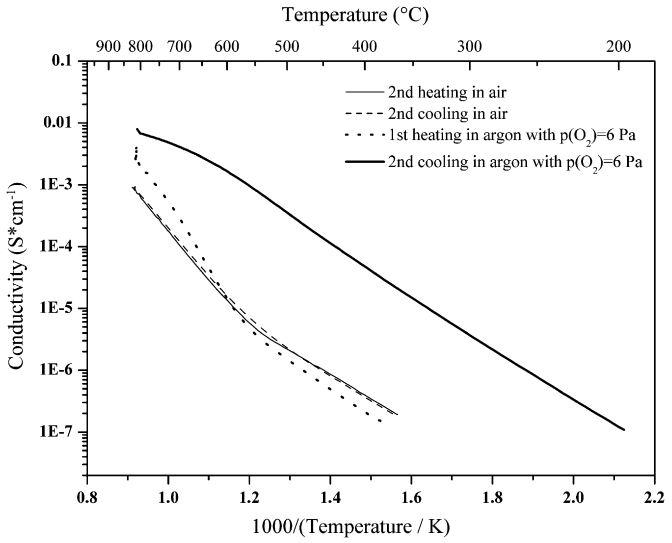

Fig. 7. Temperature dependent conductivity of VNb_9O_{25} synthesised via SCR; the sequence of sample marking corresponds to the sequence of measurements.

Table 2
Activation energies for the total electrical conductivity of $VNb_9O_{25-\delta}$, E_A (calculated from the slope of the Arrhenius plot).

Preparation	Oxygen partial pressure (Pa)	Temperature (°C)	E_A (kJ/mol)	Temperature (°C)	E_A (kJ/mol)
SSR	2.1×10^4	355–600	96	600–800	130
	2.4	230–600	97	600–800	97
	15	310–590	96	590–800	147
SCR	2.1×10^4	360–515	80	600–800	148
	6	200–660	82	660–800	56

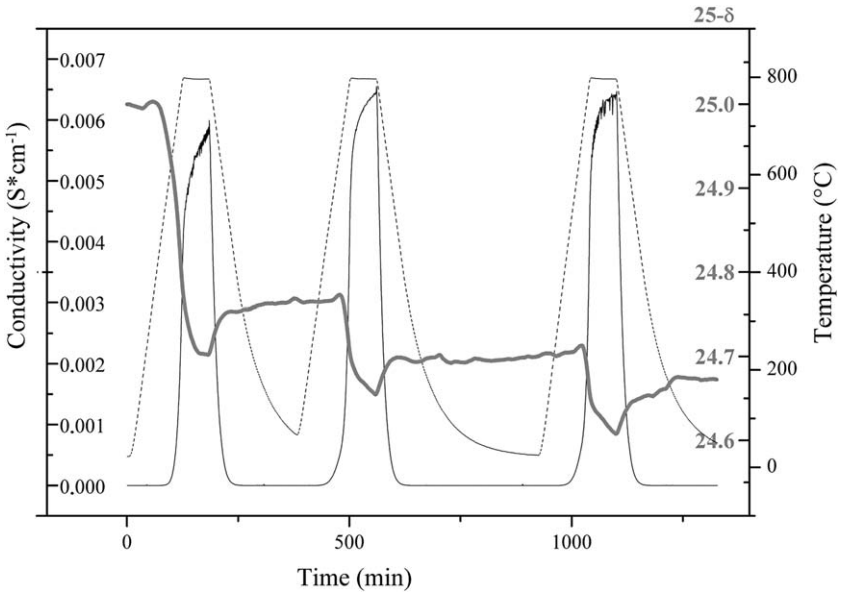

Fig. 8. Oxygen content of $VNb_9O_{25-\delta}$ measured at $p(O_2) = 2.4$ Pa (SSR, 1000 °C): temperature (gray dotted), conductivity (black, dashed) and oxygen content (black, straight).

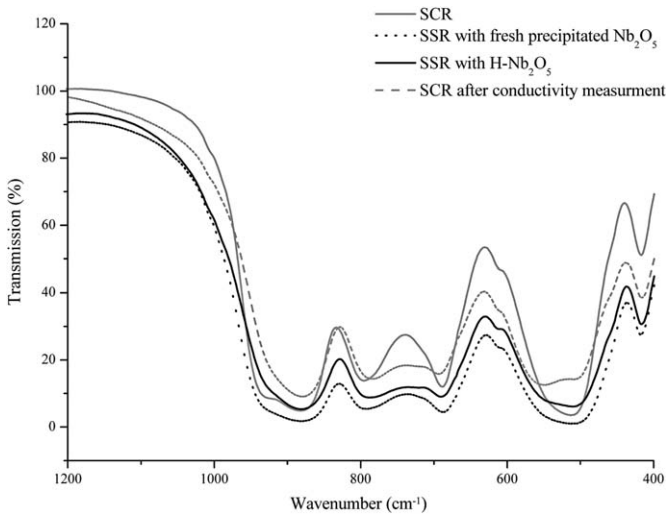

Fig. 9. IR absorption spectra of VNb_9O_{25} synthesised at 1000 °C: SCR in air (gray), SCR after conductivity measurement (gray dashed), SSR with H–Nb_2O_5 in air (black), and SSR with freshly precipitated Nb_2O_5 in air (black dashed).

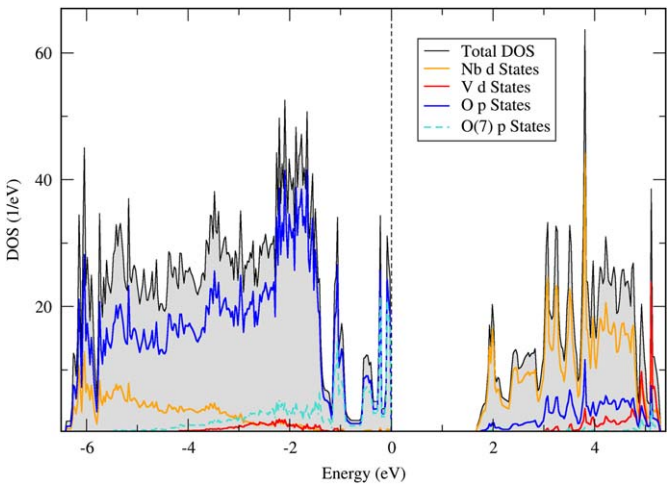

Fig. 10. DOS (density of states) of VNb_9O_{25}. Total DOS (black) and partical DOS are represented. Nb 4*d* states (orange), V 3*d* states (red), O 2*p* states (blue) O(7) 2*p* states (turquoise). The Fermi level is chosen at 0 eV.

place within a small high temperature interval. During the second and third annealing cycles a further decrease of the oxygen content can be observed, and after the third cooling process the final content at room temperature is lower than that at 800 °C during the first cycle. A return to the initial state of $VNb_9O_{25-\delta}$ with $\delta \approx 0$ requires an annealing process above 600 °C followed by a slow cooling process in air or oxygen atmosphere.

Although the results concerning the oxygen release and uptake of the powder samples described above and of sintered pills are qualitatively similar, the absolute amount of the oxygen release in an oxygen-impoverished atmosphere is higher for the powder sample. This is likely caused by the preferred oxygen loss and oxygen uptake in the shell of the compact pill. There is no change in the X-ray powder pattern after sample treatment at a low $p(O_2)$. That means that a phase transformation does not take place. However, a slight shift of some bands of the IR absorption spectra can be observed for the SCR sample (Fig. 9). The resultant IR absorption spectrum is similar to the spectra of the SSR samples. This might indicate a slight structural change. In case of low oxygen vacancy concentrations a nearly homogeneous distribution can be expected. However, for higher vacancy concentrations an inhomogeneous distribution cannot be excluded. This could result in an enrichment of vacancies at the grain surfaces. Further, the oxygen diffusion could be inhibited. While V_2O_5 is known to be easily reduced to V_nO_{2n+1}, such as V_6O_{13} [3], or, at higher temperatures, to VO_2 [1] the oxygen release from Nb_2O_5 requires a low $p(O_2)$ and high temperatures. This may hint at a preferred localisation of oxygen vacancies around the vanadium sites for $VNb_9O_{25-\delta}$.

3.6. Calculation

To closely investigate the possibility of V(IV) centres for the conductivity process, electronic structure calculations were performed. The electronic structure of VNb_9O_{25} was calculated self-consistently within the framework of the LDA to DFT. Therein, we used the linearised muffin-tin orbital (LMTO) scheme [27] in the atomic sphere approximation with combined correction terms [28]. For the exchange-correlation potential the Perdew–Wang [29] parametrisation was used. To reduce the large sphere overlap due to the loose structural packing, empty spheres were inserted.

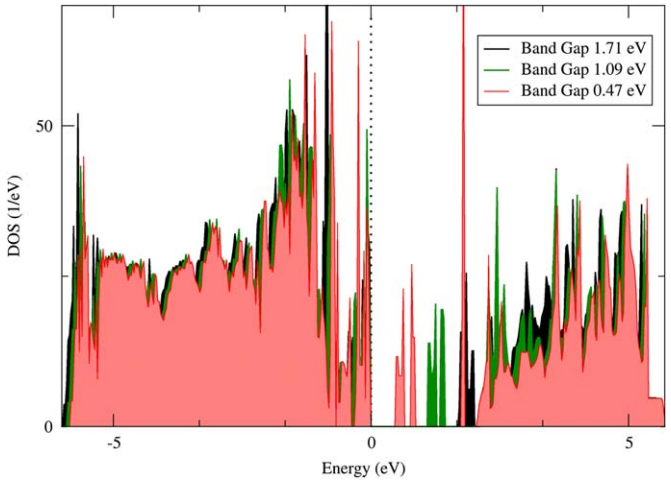

Fig. 11. DOS (density of states) of VNb_9O_{25}. Localised states of V character are appearing in the band gap on lowering the coupling between V 3*d* and O 2*p* states, explicity varying the hybridization matrix. Notice the narrowing of the band gap and the spike-like states in the gap.

Integration within the Brillouin zone on a mesh of $8 \times 8 \times 12$ k-points ensured self-consistency.

The density of states (DOS) (Fig. 10) corresponds to the one of a (*n*-type) semiconductor with a direct gap of about 1.7 eV, in agreement with calculations on binary oxides [30–32]. Vanadium 3*d* states have a dominant contribution in the higher energy region, between 3 and 5.5 eV (Fig. 10, red partial DOS). Niobium 4*d* states dominate the energy range between 1.8 and 5.0 eV (Fig. 10, orange partial DOS). The states just below the Fermi level (−1.2 to 0 eV) are mostly contributed by O(7) 2*p* states, with a much smaller V 3*d* contribution due to strong V–O hybridisation. The lower energy region (−1.5 to −6.5 eV) of the valence band (VB) is dominated by hybridised O 2*p* and Nb 4*d* states.

The partial reduction of V(V) centres to V(IV) was approached by affecting the hybridisation matrix for O(7) 2*p* states and V 3*d* states. This mimics the effect of temperature in terms of (a) an augmented effective volume for V centres due to thermal agitation and (b) a lowering of vanadium coordination by oxygen, with reduced electron transfer.

Our results are presented in Fig. 11. V(3*d*)–O(2*p*) hybridisation lowering causes localised vanadium states to appear inside the band gap. Theoretical models [33] suggest that for low mobility semiconductors, like the one in question, the Fermi level be pinned to localised states in the energy gap. The carrier conduction by hopping leads then to a thermally activated conduction behaviour of exponential form. The activation energy for this process obtained by our calculations is between 1.1 and 0.47 eV (106–45 kJmol^{-1}, green and red states in Fig. 11, respectively). These values are in good agreement with the activation energies of the measurements at lower temperature, supporting such a scenario.

3.7. Conclusions

Crystalline samples of VNb_9O_{25} can be obtained by annealing a solid state mixture of V_2O_5 and Nb_2O_5 as well as by thermal decomposition of appropriately composed freeze-dried oxalate precursors up to a temperature of 1000 °C. While the stable VNb_9O_{25} phase is formed from V_2O_5 and H–Nb_2O_5 in a direct reaction including the mineralising influence of molten V_2O_5, an annealing of the more reactive amorphous oxalate decomposition product at about 600 °C results initially in a metastable form with the structure of TT–Nb_2O_5, which is further transformed into the block structure of VNb_9O_{25} above 800 °C. In comparison with the reaction of the solid state mixtures, the reactive oxalate precursors allow the formation of crystalline samples within a shorter reaction time. Depending on the synthesis method some differences in the grain morphology are obtained (Fig. 4). However, independently of the synthesis method, the preparation of dense samples with a reproducible electrical conductivity requires a sample treatment at 1000 °C. Basically, there are no significant differences of the electrical properties of samples prepared via SSR or SCR. The good agreement allows the assumption that the conductivity values preferentially reflect the true volume conductivity and grain size and grain surface influences are of minor importance.

All samples exhibit *n*-type conductivity of hopping type with a preferred localisation of charge carriers at vanadium (V^{4+}) sites. Because of the inhibited oxygen deficiency changes at lower temperature, the electrical conductivity strongly depends on the history of the sample. The faster the rate of a preceding cooling process and the lower the $p(O_2)$ during this process, the higher is the frozen charge carrier concentration at room temperature. Between room temperature and about 600 °C the activation energy for the total electrical conductivity displays a thermally activated hopping behaviour. Experimental and calculated values agree well. Above 600 °C the thermally activated hopping process is superimposed by a $p(O_2)$-dependent oxygen release. This results in a stronger increase of conductivity and, formally, an increase of the measured activation energy.

Acknowledgments

The authors would like to thank P. Scheppan and U. Burkhardt for SEM measurements. We thank Prof. U. Guth for support in conductivity measurements and powder characterisation. We also want to thank L. Craco for helpful discussions. We acknowledge the Deutsche Forschungsgemeinschaft (DFG) for financial support.

References

[1] W. Brückner, H. Oppermann, W. Reichelt, J.I. Terukow, F.A. Tschundnowski, E. Wolf, Vanadiumoxide, Akademie Verlag, Berlin, 1983.
[2] N. Kumagai, K. Tanno, T. Nakajima, N. Watanabe, Electrochim. Acta 28 (1983) 17–22.
[3] J.H. Perlstein, J. Solid State Chem. 3 (1971) 217–226.
[4] C. Zhao, I.E. Wachs, Catal. Today 118 (2006) 332–343.
[5] I.E. Wachs, Y. Chen, J.M. Jehng, L.E. Briand, T. Tanaka, Catal. Today 78 (2003) 13–24.
[6] W. Chen, Y. Kaneko, N. Kinomura, J. Appl. Electrochem. 32 (2003) 515–518.
[7] P. Moggi, M. Devillers, P. Ruiz, G. Predieri, D. Cauzzi, S. Morselli, O. Ligabue, Catal. Today 81 (2003) 77–85.
[8] M. Cherian, M.S. Rao, G. Deo, Catal. Today 78 (2003) 397–409.
[9] H. Schadow, H. Oppermann, O. Grossmann, Cryst. Res. Technol. 27 (1996) 835–838.
[10] H.J. Goldschmidt, Metallurgia 18 (1960) 211–218.
[11] J.L. Waring, R.S. Roth, Acta Cryst. 17 (1964) 455.
[12] R.S. Roth, A.D. Wadslay, Acta Cryst. 18 (1965) 643–647.
[13] M.T. Casais, E. Gutierrez-Puebla, M.A. Monge, I. Rasines, C. Riuz-Valero, J. Solid State Chem. 102 (1993) 261–266.
[14] O. Yamaguchi, Y. Mukaida, H. Shigeta, Adv. Powder Technol. 1 (1990) 3–12.
[15] T. Mayer-Uhma, H. Langbein, Thermochim. Acta 447 (2006) 178–183.
[16] J.M. Amarilla, B. Casal, E. Ruiz-Hitzky, J. Mater. Chem. 6 (1996) 1005–1011.
[17] H. Langbein, T. Mayer-Uhma, Mater. Res. Bull. 44 (2009) 654–659.
[18] A. Amoutza, F. Riza, V. Kasselouri, Mater. Lett. 57 (2003) 2298–2304.
[19] P. Kofstad, J. Phys. Chem. Solids 23 (1962) 1571–1578.
[20] H. Langbein, S. Christen, G. Bonsdorf, Thermochim. Acta 327 (1999) 173–180.
[21] L.A. Simpson, R.E. Carter, J. Am. Ceram. Soc. 49 (1966) 139–144.
[22] F.F.P. Medeiros, M.F.V. Moura, A.G.P. da Silva, C.P. Souza, K.K.P. Gomes, U.U. Gomes, Braz. J. Chem. Eng. 23 (2006) 531–538.
[23] M.A. Bizeto, V.R.L. Constantino, Eur. J. Inorg. Chem. (2007) 579–584.
[24] R.A. Chalmers, R.W.E. Watts, Analyst 97 (1972) 224–232.
[25] A. Polte, H. Langbein, Z. Anorg. Allg. Chem. 620 (1994) 1947–1952.
[26] E.V. Arkhipova, M.G. Zuev, L.A. Perelyaeva, J. Alloys Compd. 414 (2005) 48–54.
[27] O.K. Andersen, Phys. Rev. B 12 (1975) 3060–3083.
[28] O.K. Andersen, O. Jepsen, D. Glötzel, in: F. Bassani, F. Fumi, M.P. Tosi (Eds.), Highlights of Condensed Matter Theory, North-Holland, New York, 1985.
[29] J.P. Perdew, Y. Wang, Phys. Rev. B 45 (1992) 13244–13249.
[30] S. Atzkern, S.V. Borisenko, M. Knupfer, M.S. Golden, J. Fink, Phys. Rev. B 61 (2000) 12792–12798.
[31] R.J.O. Mossanek, A. Mocellin, M. Abbate, B.G. Searle, P.T. Fonseca, E. Morikawa, Phys. Rev. B 77 (2008) 075118.
[32] Q.H. Wu, A. Thissen, W. Jaegermann, M. Schüz, P.C. Schmidt, Chem. Phys. Lett. 430 (2006) 309.
[33] C.H. Karakotsou, J.A. Kalomiros, M.P. Hanias, A.N. Anagnostopoulos, J. Spyridelis, Phys. Rev. B 45 (1992) 11627–11631.